ImmunoTargets and Therapy

Dovepress
Taylor & Francis Group

Open Access Full Text Article

ORIGINAL RESEARCH

The Dual Mechanism of Action of CO-005 Overcomes CD20 Resistance in Diffuse Large B-Cell Lymphoma

Sittana Matar[1,2], Seham Skah[1], Liza EB Moltu[1], Øystein Åmellem[1], Hanne R Hagland[2], Kjetil Hestdal[1], Rolf D Pettersen[1], Nina Richartz[1]

[1]Caedo Oncology AS, Oslo, Norway; [2]Department of Chemistry, Bioscience and Environmental Engineering, University of Stavanger, Stavanger, Norway

Correspondence: Sittana Matar, Caedo Oncology AS, Oslo, Norway, Tel +4745392734, Email sittanamatar@gmail.com

Purpose: Despite the clinical success of anti-CD20 monoclonal antibodies (mAbs) such as rituximab in the treatment of B-cell lymphoma, therapeutic resistance and relapse remain significant challenges, particularly in tumors with low or heterogeneous CD20 expression resulting from antigen loss or phenotypic shifts. To address this limitation, new therapeutic strategies are needed that act independently of CD20 while maintaining robust immune effector engagement. CO-005 is a humanized anti-CD47 fusion protein designed to simultaneously disrupt the CD47–SIRPα checkpoint and induce direct programmed cancer cell death (PCCD) distinct from other anti-CD47 agents.

Methods: The capacity of therapeutic mAbs to induce PCCD was assessed in lymphoma cell lines by flow cytometric detection of cell death and apoptotic markers. Antibody binding, phagocytic activity, and mechanistic analyses assessed intracellular signaling events associated with PCCD were measured by flow cytometry following treatment. The antitumor activity of CO-005 was evaluated in NOD-scid IL2Rγnull (NSG) mice bearing subcutaneous lymphoma xenografts, with efficacy and survival outcomes assessed for CO-005 as monotherapy and in combination with rituximab.

Results: CO-005 demonstrated potent and durable antitumor activity across multiple lymphoma xenograft models, including rituximab-resistant tumors model. CO-005 shares key mechanistic features with therapeutic anti-CD20 antibodies independent of CD20 signaling, including the induction of type III programmed cell death via receptor capping, calcium flux, reactive oxygen species generation, and actin cytoskeleton dependence, accompanied by surface calreticulin exposure. In vivo, CO-005 triggered robust intratumoral PCCD and remodelled the tumor microenvironment, characterized by increased macrophage and neutrophil infiltration, thereby enhancing innate immune activation and supporting a dual-mechanism mode of action that couples direct cancer cell killing with myeloid engagement.

Conclusion: These findings position CO-005 as a mechanistically distinct and immunologically active therapeutic with the potential to overcome limitations of both CD20- and CD47-directed therapies and expand treatment options for B-cell lymphoma.

Keywords: B cell lymphoma, anti-CD47 fusion protein, rituximab resistance, CD20 antigen loss, PCCD, immunotherapy

Introduction

Anti-CD20 mAbs have improved the therapeutic landscape of B-cell non-Hodgkin lymphomas (B-NHL), establishing new standards of care across disease stages.[1,2] Rituximab (RTX), in particular, forms the immunologic backbone of standard chemoimmunotherapy regimens such as R-CHOP (rituximab, cyclophosphamide, doxorubicin, vincristine, and prednisone), which remains the frontline treatment for diffuse large B-cell lymphoma (DLBCL).[3] In this setting, RTX synergizes with cytotoxic agents to drive tumor regression. However, a significant proportion of patients fail to respond or relapse early, often due to immune evasion and antigen escape, which compromise both the antibody and chemotherapy components of the regimen.[4,5] These challenges underscore the need for improved immunotherapeutic strategies that bypass CD20 dependence and adding intrinsic cytotoxic activity, immune checkpoint inhibition, and immune activation in targeting lymphomas.

https://doi.org/10.2147/ITT.S572396
Received: 8 October 2025
Accepted: 23 January 2026
Published: 19 February 2026

Resistance to anti-CD20 therapy arises through multiple mechanisms, including impaired Fc receptor signaling, depletion or dysfunction of effector cells, and compensatory upregulation of alternative immune checkpoints such as CD47.[6,7] In addition, CD20 expression is heterogeneous across B-NHL subtypes and may be dynamically lost following treatment, rendering a subset of tumors partially or completely refractory to CD20-directed therapies.[8]

CD47, often termed the "don't eat me" signal, is a transmembrane protein that binds signal regulatory protein α (SIRPα) on macrophages and neutrophils, suppressing phagocytic clearance of malignant cells.[9,10] Its overexpression in a range of cancers, including B-NHL, confers immune evasion and is associated with poor prognosis.[11,12] While CD47 blockade has shown promise in preclinical models and early clinical trials, most agents rely on antibody-dependent phagocytosis and require co-administration with cytotoxic or opsonizing antibodies to achieve full efficacy[13,14] By contrast, recent studies have identified a subset of anti-CD47 antibodies that induce direct, caspase-independent cell death characterized by phosphatidylserine (PS) exposure, reminiscent of type II anti-CD20 antibodies such as obinutuzumab (OBZ).[15,16] These "non-classical" death pathways, referred to as type III programmed cell death, are increasingly recognized as immunogenic and may contribute to therapeutic responses beyond conventional apoptosis.[17]

Importantly, growing evidence supports functional synergy between CD47 and CD20 targeting. CD47 blockade has been shown to enhance rituximab-mediated phagocytosis and may restore responsiveness in rituximab-refractory disease.[18,19] Within DLBCL subtypes, molecular subtypes exhibit distinct immunobiological features that may influence therapeutic sensitivity. The activated B-cell–like (ABC) subtype, for example, has been associated with elevated CD47 expression and increased reliance on innate immune evasion mechanisms, potentially rendering it more susceptible to CD47-targeted strategies.[20] In contrast, the germinal center B-cell–like (GCB) subtype—though generally more responsive to standard immunochemotherapy[21] may still benefit from CD47 blockade in settings of relapse or resistance. Together, these findings support a therapeutic strategy that targets CD47 through both immune checkpoint disruption and direct cytotoxicity to overcome key limitations of CD20-based regimens.

Here, we investigate CO-005[14] a bivalent humanized single-chain variable fragment–fragment crystallizable (scFv-Fc) fusion protein, uniquely engineered to simultaneously block the CD47–SIRPα axis and induce rapid PCCD. By integrating immune checkpoint disruption with direct cytotoxicity, CO-005 represents a mechanistically novel approach that has the potential to overcome resistance to CD20-targeted therapies. This dual-function design expands the therapeutic scope in B-cell lymphomas, which may offer opportunities for both monotherapy and rational combination regimens aimed at improving response rates and durability across resistant or immunologically cold disease settings.

Materials and Methods

Antibodies and Isotype Controls

The humanized anti-CD47 fusion protein, CO-005, was produced at ATUM (Newark, CA, USA) as previously described.[14] The anti-CD47 monoclonal antibody (2D3) was purchased from Thermo Fisher Scientific (cat# 14–0478-82). The anti-CD20 monoclonal antibody rituximab (MabThera) was from Roche. CD20 (obinutuzumab) recombinant human monoclonal antibody (GA101) was purchased from Thermo Fisher Scientific (Cat# LT906-1MG). Human IgG4κ isotype control antibodies were purchased from Sino Biological (Cat# HG4K), and mouse IgG1 chimeric isotype control (MOPC-21) was obtained from Thermo Fisher Scientific (Cat# MA5-47824). All experiments presented in this study were performed using the same antibody batch.

Cell Line and Culture Conditions

A panel of B-cell lymphoma cell lines representing distinct subtypes was used in this study. Daudi (CCL-213), Raji (CCL-86), SU-DHL-6 (CRL-2959), and NU-DUL-1 (CRL-2969) were purchased from the American Type Culture Collection (ATCC, USA). ULA (ACC-267), Riva (ACC-585), OCI-LY18 (ACC-699), OCI-LY19 (ACC-528), and SU-DHL-10 (ACC-576) were obtained from the Leibniz Institute DSMZ–German Collection of Microorganisms and Cell Cultures (DSMZ). The classification, origin, and culture conditions for each cell line are summarized in Supplementary Table S1. Cells were cultured in the appropriate media supplemented with 10–20% (v/v) fetal bovine serum (FBS, Cat# ESC5000L) and 1% (v/v) penicillin-streptomycin (Thermo Fisher Scientific, Cat# 15140122). RPMI-1640 medium (Cat#

EC-ECB2000L) was from EuroClone, Iscove's Modified Dulbecco's Medium (IMDM; Cat# 12440053), Opti-MEM (Cat# 31985070), and alpha-MEM (Cat# 12571063) were purchased from Thermo Fisher Scientific. All cells were cultured in a humidified incubator at 37 °C with 5% CO_2 and 95% air. Cells were routinely tested for mycoplasma contamination and authenticated by flow cytometry.

Antibody Binding Assay and Receptor Quantification

PBS-washed lymphoma cancer cells or normal B cells ($5x10^5$ cells/mL) were resuspended in blocking buffer (10% (v/v) FBS, 1% (w/v) sodium azide (NaN_3) in phosphate-buffered saline (PBS)), then incubated with 10 µg/mL of CO-005, RTX, or OBZ on ice for 1 h with gentle agitation. Each sample was prepared in duplicate. Cells were then washed twice at 500 ×*g* for 5 min at 4°C in washing buffer (w/v) BSA, 1% (w/v) NaN_3 in PBS), then resuspended in blocking buffer containing 5 µg/mL PE-conjugated goat anti-human IgG Fc secondary antibody (Thermo Fisher Scientific, Cat# 12–4998-82) and incubated on ice for 30 min with slight agitation. The cells were then washed three times with cold washing buffer and analyzed by flow cytometry on a MACSQuant X (MQX, Miltenyi Biotec) equipped with three lasers (405, 488, 640 nm) and eight detection channels. Excitation wavelength for PE was 488 nm and detection wavelength 585/40nm. Receptor quantification of CD20 and CD47 was performed by using the PE-conjugated calibration beads (BD Biosciences, Cat# 340495). The PE-beads were run in parallel to the binding assay to estimate the number of CD20 and CD47 molecules expressed on the lymphoma cancer cell surface.

Cell Death Assay

Cell death was assessed using Annexin V eFluor™ 450 and 7-AAD staining, following the manufacturer's instructions (Thermo Fisher Scientific, Cat# 88–8006-74). Briefly, 5×10^5 cells/mL were either left untreated (control) or treated with 1 µg/mL of CO-005, RTX, OBZ, and human IgG isotype control (IgG4 or IgG1), and incubated for either 3 or 24 hours. Cells were then stained and immediately analyzed by flow cytometry using the MQX. Annexin V was excited at 405 nm and detected at 450/50 nm, while 7-AAD was excited at 488 nm and detected between 655–730 nm. % PCCD represents the sum of early apoptotic (Annexin V^+ 7-AAD^-) and late apoptotic (Annexin V^+ 7-AAD^+) cell populations.

Immunofluorescence and Confocal Microscopy

Lymphoma cancer cells (5×10^5 cells/mL) were treated with 1µg/mL of CO-005, RTX, or OBZ for 3 or 24 hours. Following treatment, cells were washed, fixed with 4% paraformaldehyde (PFA) in PBS for 15 minutes, and permeabilized with 0.2% Triton X-100 for 30 minutes at room temperature. Blocking was performed with 20% goat serum or 1% bovine serum albumin (BSA) in PBS for 20 minutes. Cells were incubated overnight at 4 °C with the anti-CD47 monoclonal antibody (2D3), followed by a 2-hour incubation at room temperature with Alexa Fluor 488-conjugated goat anti-mouse IgG. CD20 was detected using Alexa Fluor 647-conjugated goat anti-human IgG (Thermo Fisher Scientific, Cat# A48279). Stained cells were transferred to 8-well chambered borosilicate cover glass slides (Nunc), mounted using ProLong™ Gold Antifade Mountant with DNA Stain DAPI (Thermo Fisher Scientific, Cat# P36931), and imaged in PBS. Bright-field and fluorescence images were acquired on a Zeiss LSM 880 confocal microscope using a 63× oil immersion objective (laser power 5%, detector gain 600nm). Images were merged using Fiji: ImageJ software.[22]

Calreticulin Surface Exposure Assay

Lymphoma cell lines were seeded at 5×10^5 cells/mL and treated in duplicate with CO-005, RTX, and OBZ for 3 or 24 hours. Doxorubicin (Sigma-Aldrich Cat#D1515) served as a positive control for calreticulin exposure (2µg/mL). Following treatment, cells were washed twice and resuspended with flow cytometry staining buffer (PBS + 2% FBS), containing Alexa Fluor® 405 Anti-Calreticulin antibody anti-calreticulin antibody [EPR3924] - ER Marker (Abcam, Cat# ab210431, dilution 1:100). The samples were incubated on ice for 40 minutes with gentle agitation, then washed twice with 150 µL staining buffer. Cells were finally resuspended in 200 µL staining buffer for acquisition. For samples not treated with doxorubicin, 7-AAD (BioLegend, Cat# 420403; final concentration 25 µg/mL) was added for live/dead discrimination. Flow cytometric analysis was performed on the MQX. Alexa Fluor 405 excitation/detection: 401/421 nm; 7-AAD excitation/detection: 488/650 nm. Calreticulin positivity was assessed as the percentage of calreticulin positive

live cells and/or by median fluorescence intensity (MFI), normalized to untreated controls. All experiments were independently repeated at least three times (n= 3) by different users.

Cellular Stress Profiling via Calcium Flux, Reactive Oxygen Species, Mitochondrial Potential, and Actin Polarization Assays

Lymphoma cells were assessed for intracellular calcium flux, reactive oxygen species (ROS) generation, and mitochondrial membrane potential (MMP) changes using Fluo-4 AM, CellROX Green, and tetramethylrhodamine methyl ester (TMRM). Lymphoma cell lines were seeded at 6×10^5 cells/mL in 3 mL volumes per condition and treated in duplicate with (1μg/mL) of CO-005, RTX, OBZ or isotype control for 3 hours at 37°C in a humidified 5% CO_2 incubator. At the end of treatment, cells were split into three aliquots: 500 μL for CellROX, and 1 mL each for TMRM and Fluo-4 assays.

For the TMRM assay, cells were incubated with 20 nM TMRM (Thermo Fisher Scientific, Cat# T668) for 30 minutes at 37°C, 5% CO_2. As a positive control for mitochondrial depolarization, cells were treated with 50 μM carbonyl cyanide m-chlorophenyl hydrazone (CCCP) for 5 minutes under the same conditions.[23]

After staining, 200 μL of each sample was transferred to a 96-well round-bottom plate and analyzed on a MACSQuant X flow cytometer (Miltenyi Biotec) using the PE channel (excitation 488 nm, emission 585/40 nm). Loss of MMP was indicated by decreased TMRM fluorescence ($TMRM^{low}$ population).

ROS were detected using CellROX Green reagent (Thermo Fisher Scientific, Cat# C10444). Cells were incubated for 30 minutes at 37°C with 5 μM CellRox Green. After staining, cells were washed once and resuspended in 200 μL PBS. Samples were transferred to a 96-well round-bottom plate and analyzed on the MQX (excitation 488 nm, emission 530/30 nm).

Intracellular calcium levels were measured using Fluo-4 AM (Thermo Fisher Scientific, Cat# F14201). Fluo-4 was added to cell suspensions at a final concentration of 5 μM, followed by 30-minute incubation at 37°C. Cells were then washed once and resuspended in HBSS buffer supplemented with 1 mM glucose. A further 30-minute incubation at room temperature allowed for complete de-esterification of the acetoxymethyl ester (AM) groups. 200 μL of each sample was transferred to a 96-well round-bottom plate and analyzed by flow cytometry on the MQX (excitation 488 nm, emission 530/30 nm).

For inhibitor of actin polymerization experiment, NU-DUL-1 cells were pre-treated with 20 μM cytochalasin D for 15 minutes in a standard cell culture incubator (37 °C, 5% CO_2, humidified atmosphere). Following pre-treatment, cells were incubated with 1 μg/mL of CO-005, OBZ, or isotype control for 3 hours under standard cell culture conditions. Annexin V and 7-AAD staining were then performed as described above.

Lymphoma Xenograft Models

Lymphoma xenograft models using NU-DUL-1, Daudi, OCI-LY19, and Raji cell lines were established by washing the cells and resuspending them at 1.5×10^6 cells per 0.1 mL in a 1:2 PBS:Vitrogel mixture (TheWell Bioscience, Cat# VHM01), followed by subcutaneous (SC) injection into mice into the right flank of 6-8-weeks old female NOD-scid IL2Rγnull (NSG) mice (The Jackson Laboratory, Strain #005557). Treatments were initiated once tumors reached an average volume of 150 mm^3. Tumor volume was measured in two dimensions (length and width), using a standard caliper by an investigator blinded to the treatment groups, and calculated using the formula: tumor volume = (length × $width^2$) / 2. Following establishment of measurable tumors, mice were randomized into treatment groups. Each treatment group was housed within a single cage. For the NU-DUL-1 and OCI-LY19 xenograft studies, six mice were assigned to each treatment group, while for the Daudi model, five mice were assigned per group. Treatments were administered by intraperitoneal (i.p) injections twice weekly for three consecutive weeks. Tumor volume, body weight, and survival were recorded throughout the study. In the Raji xenograft model, three mice per group received a single-dose treatment.

Single-Cell Analysis of Tumor-Infiltrating Myeloid and Apoptotic Cells

A xenograft model of Burkitt's lymphoma using the Raji cell line was established as described above. On day 10 post-inoculation, mice were divided into two groups: an untreated control group (n=2) and a treatment group receiving a single intraperitoneal injection of CO-005 at 5 mg/kg (n=3). Three days post-treatment, mice were euthanized, and tumors were collected for downstream analysis.

Tumors were dissociated into single-cell suspensions using the Tumor Dissociation Kit and gentleMACS Dissociator (Miltenyi Biotec Cat# 130–095-929), following the manufacturer's instructions. Cell suspensions were centrifuged at 500 ×*g* for 5 minutes, resuspended in PBE buffer (PBS with 2 mM EDTA and 0.5% BSA), and counted.

For flow cytometric analysis, cells were stained on ice with mouse F4/80 monoclonal antibody (BM8), eFluor™ 450 (Thermo Fisher Scientific, Cat# 48–4801-82) or mouse Ly-6G/Ly-6C monoclonal antibody (RB6-8C5), PE (Thermo Fisher Scientific, Cat# 12–5931-82), using 5 µL antibody in 100 µL PBE per sample and incubated for 20 minutes. Stained cells were washed twice (500 ×*g*, 6 minutes, 4°C), resuspended in PBE, and analyzed using the MQX flow cytometer (excitation 488 nm, emission 585/40 nm for PE; excitation: 405nm, emission: 445 nm for eFluor 450). Apoptotic cells were identified using Annexin V and 7-AAD staining as described above.

Ethical Statement

All animal experiments were conducted in accordance with institutional and national guidelines for the care and use of laboratory animals. Protocols were reviewed and approved by the Norwegian Food Safety Authority (approval ID: 29016). The in vivo studies were performed between [April 2024] and [May 2025]. Mice were housed under specific pathogen–free conditions with ad libitum access to food and water, and their health status was monitored daily. Humane endpoints were predefined: animals were euthanized when tumor volume reached 2000 mm^3, if ulcerations developed at the tumor site, or if symptoms exceeded a predetermined humane endpoint. Euthanasia was performed in compliance with institutional standard operating procedures to minimize suffering. We have adhered to ARRIVE guidelines on reporting of animal in vivo experiments.

Phagocytosis Assay

RAW264.7 murine macrophages were seeded in 6-well plates at 4×10^5 cells per well and allowed to adhere overnight at standard cell culture conditions. Cells were then stained with 40 nM Vybrant™ DiO (Thermo Fisher Scientific Cat# V22886) for 20 minutes at 37°C, followed by three washes with DMEM. Target cancer lymphoma cells were stained with CellTrace™ Violet (Thermo Fisher Scientific Cat# C34557) according to the manufacturer's protocol and added to the macrophages along with antibody treatments. After 2 hours of incubation at 37°C, cells were scraped and washed twice with PBS containing 1 mM EDTA and analyzed by flow cytometry on the MQX. Phagocytosis was quantified as the percentage of cells double positive for DiO and CellTrace Violet, indicating engulfment of target cells by macrophages, as previously described.[14] Excitation wavelength DiO: 488nm, detection wavelength: 525/50 nm, excitation wavelength CellTrace Violet: 405 nm, detection wavelength: 450/50 nm.

Statistical Analysis

Statistical analysis was performed using GraphPad Prism 9 (GraphPad Software Inc). Unless stated otherwise, all experiments were conducted with a minimum of three independent replicates. Error bars represent the standard deviation (S.D)., and statistical analyses were performed using analysis of variance (ANOVA). To determine the statistical differences between different animal treatment groups, the Mann–Whitney *U*-test was employed. All statistical tests were two-sided, followed by Tukey's multiple comparisons test and the significance level was set to 5% ($p<0.05$), unless otherwise stated.

Results

CO-005 Induces Potent Cell Death in DLBCL Independent of CD47 Expression Levels

To evaluate the activity of CO-005 in comparison with clinically established anti-CD20 antibodies—RTX (type I) and OBZ (type II)—we first characterized a panel of DLBCL cell lines by flow cytometry for surface expression of CD47 and CD20. The panel included ABC-subtype cell lines (NU-DUL-1, Riva, SU-DHL-2, OCI-LY18) and GCB-subtype cell lines (SU-DHL-6, SU-DHL-10, OCI-LY19),[21] two well-characterized Burkitt lymphoma cell lines (Raji and Daudi),[24] and one unclassified DLBCL cell line ULA.[25] Antibody binding capacity was quantified using standardized calibration beads conjugated to four different levels of phycoerythrin (PE). As shown in Figure 1A (left panel), CD47 expression varied widely across the tested DLBCL cell lines, indicating substantial heterogeneity. While high CD47 levels were

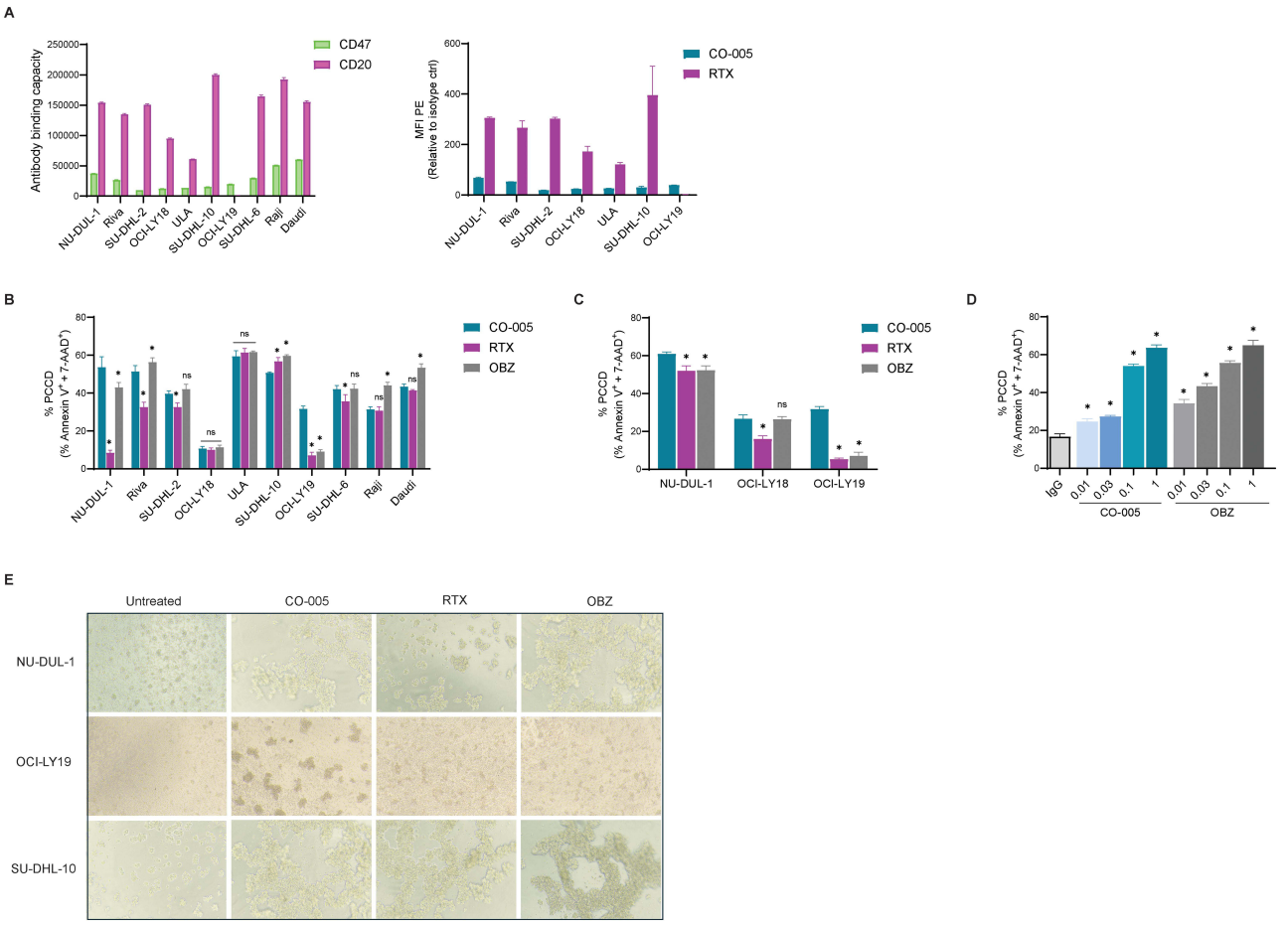

Figure 1 CO-005 induces potent cell death in DLBCL independent of CD47 expression levels. **(A)** Antibody binding capacity of CO-005 (anti-CD47) and rituximab (RTX; anti-CD20) in lymphoma cell lines. Left panel: Quantification of antibody binding capacity using PE-conjugated anti-human Fc secondary antibody and PE calibration beads. Right panel: Relative antibody binding across selected cell lines normalized to IgG isotype control. **(B** and **C)** Lymphoma cell lines treated with CO-005, RTX, or OBZ for **(B)** 3hours, or **(C)** 24 hours. **(D)** NU-DUL-1 cell line treated with 0.01–1 μg/mL CO-005 or OBZ for 3 hours. Cell death was determined by Annexin V and 7-AAD staining and analyzed by flow cytometry. Data represent the mean ± SD. Significance was determined by ANOVA analysis *, $P < 0.01$ relative to the sample treated with CO-005; ns indicates not significant. All experiments were performed independently three times (n = 3). MFI, mean fluorescence intensity. **(E)** Representative bright-field microscopy images (20×) of homotypic cell aggregation in lymphoma cell lines after 3-hour treatment with indicated antibodies.

more frequently observed in ABC subtypes such as NU-DUL-1 and Riva, consistent with previous reports,[26] elevated expression was not exclusive to this group, as it was also detected in the GCB cell line SU-DHL-6. All cell lines expressed CD20; however, OCI-LY19 showed very low levels, approaching a CD20-negative profile (Figure 1A, left panel). The binding activity of CO-005 and RTX in selected cell lines is also shown (Figure 1A, right panel).

Next, we assessed the cytotoxic activity of CO-005 in vitro across the panel of lymphoma cell lines and compared its activity to RTX and OBZ. Obinutuzumab (OBZ) has previously been shown to induce direct PCCD and demonstrate superior therapeutic efficacy over RTX in preclinical models of DLBCL.[27] As shown in Figure 1B, short-term incubation (3 hours) with CO-005 or OBZ at 1 μg/mL resulted in robust cell death in multiple cell lines, including NU-DUL-1, Riva, SU-DHL-2, ULA, SU-DHL-6, SU-DHL-10, Daudi, and Raji, measured by Annexin V and 7-AAD staining (Figure 1B). RTX also induced cell death in a subset of these cell lines under the same conditions, though generally to a lesser extent. In NU-DUL-1 cells, CO-005 and OBZ induced rapid and saturable cell death, with maximal effects observed as early as 3 hours and no significant increase by 24 hours (Figure 1B and C). This cytotoxic activity was also dose-dependent (Figure 1D). In contrast, RTX required prolonged incubation—up to 24 hours—to reach comparable levels of cell death in this cell line (Figure 1C). In OCI-LY18 cells, RTX showed limited cytotoxic activity even after 24 hours of exposure, whereas both CO-005 and OBZ were more effective (Figure 1C). Notably, OCI-LY19 cells, which express minimal CD20,[28] were unresponsive to RTX and OBZ but remained sensitive to CO-

005, further supporting a CD20-independent mechanism of action (Figure 1C). The cell death was also associated with cell aggregation, characterized by the formation of dense cellular clusters and loss of uniform distribution, as observed by light microscopy (Figure 1E).

CO-005 Triggers Receptor Capping and Signaling Events Associated with Type I and II Anti-CD20 Antibodies

Given that CO-005 induces direct PCCD in a manner apparently similar to OBZ and RTX, we investigated whether CO-005 ligation of CD47 shares mechanistic features with CD20 ligation with type I and II mAbs. Using confocal microscopy, we observed that CO-005 induced prominent redistribution of CD47 into a polarized cap-like structure at one side of the cell membrane in all tested responsive DLBCL cell lines (Figure 2A–D). This reorganization occurred rapidly within minutes of exposure (data not shown) and was comparable in pattern to CD20 capping induced by RTX.[29] OBZ, while classically considered non-capping,[30] also induced detectable CD20 redistribution in some responsive cell lines (NU-DUL-1 and ULA) (Figure 2A and B), although to a lesser extent than RTX or CO-005 in the SU-DHL-10 cell line (Figure 2C). In CD20-low OCI-LY19 cells, CO-005 induced CD47 capping, whereas RTX and OBZ failed to trigger CD20 capping despite visible surface expression (Figure 2D), suggesting a threshold of CD20 density may be required for this process. Similarly, CO-005 triggered capping in CD20-negative Jurkat cells, confirming that the phenomenon is independent of CD20 expression (Supplementary Figure S1A). In contrast, CD47-binding antibodies that do not induce PCCD—magrolimab and B6H12—did not elicit CD47 capping (Supplementary Figure S1 A), supporting a direct mechanistic link between receptor reorganization and the PCCD mediated by CO-005. CO-004, a single-chain variable fragment (scFv) version of CO-005 that retains the cytotoxic activity of the full-length antibody,[14] also induced CD47 capping, indicating that redistribution is Fc-independent and intrinsic to the CO-005–CD47 interaction (Supplementary Figure S1A). CO-005 similarly triggered CD47 capping in additional T- and B-ALL cell lines—MOLT-4 and Reh, respectively—both previously shown to be responsive to CO-005–mediated cell death,[14] whereas unresponsive AML cells such as KG-1a[14] lacked capping (Supplementary Figure S1B), further supporting the association between capping and functional susceptibility, and indicates that CD47 capping is an early event likely required for CO-005–mediated tumor cell death.

Calcium signaling, ROS generation, mitochondrial stress, and actin cytoskeletal remodeling have been implicated as key intracellular events in anti-CD20-mediated programmed cell death;[16,31] therefore, to determine whether CO-005 engages similar pathways, we treated a panel of CO-005–responsive DLBCL cell lines (NU-DUL-1, ULA, SU-DHL-10, and OCI-Ly19) with CO-005, RTX, or OBZ at 1 μg/mL for 3 hours followed by analysis of these downstream responses. In all tested CO-005 PCCD responsive cell lines, CO-005 induced a rapid increase in intracellular calcium levels, comparable to those triggered by RTX and OBZ (Figure 2E). RTX elicited a weaker response in NU-DUL-1 cells, aligning with its delayed cytotoxic activity in this line. In OCI-LY19, RTX and OBZ induced modest increase in calcium flux, suggesting this signal may correlate with PCCD sensitivity (Figure 2E). As shown in Figure 2F, CO-005 triggers ROS generation in the two tested cell lines. In NU-DUL-1 cells, OBZ induced the highest ROS levels relative to isotype control group, followed by CO-005, while RTX showed minimal effect. In contrast, SU-DHL-10 cells responded strongly to all three antibodies, with comparable increases in CellROX fluorescence (~2-fold over isotype control). Further, CO-005 treatment did not disrupt mitochondrial membrane potential in NU-DUL-1, as measured by TMRM staining (Figure 2G).[15] Finally, we investigated the role of the actin cytoskeleton. Pre-treatment of NU-DUL-1 cell line with cytochalasin D significantly reduced PCCD in CO-005– and OBZ-treated cells (Figure 2H), implicating actin remodeling as a shared requirement for cell death execution in type II-antiCD20 mAb.[16]

CO-005 Shifts the Phagocytic Balance by Inhibiting CD47 and Enhancing "Find Me" and "Eat Me" Signals

Having established that CO-005 induces PCCD characterized by phosphatidylserine (PS) exposure, we next investigated whether this death process involves additional features of immunogenic cell death. Specifically, we assessed the cell surface exposure of the damage associated molecular pattern (DAMP) molecule calreticulin, a key "eat me" signal that facilitates recognition and engulfment by phagocytes.[32] To assess the ability of CO-005 to induce pro-phagocytic signals,

https://doi.org/10.2147/ITT.S572396

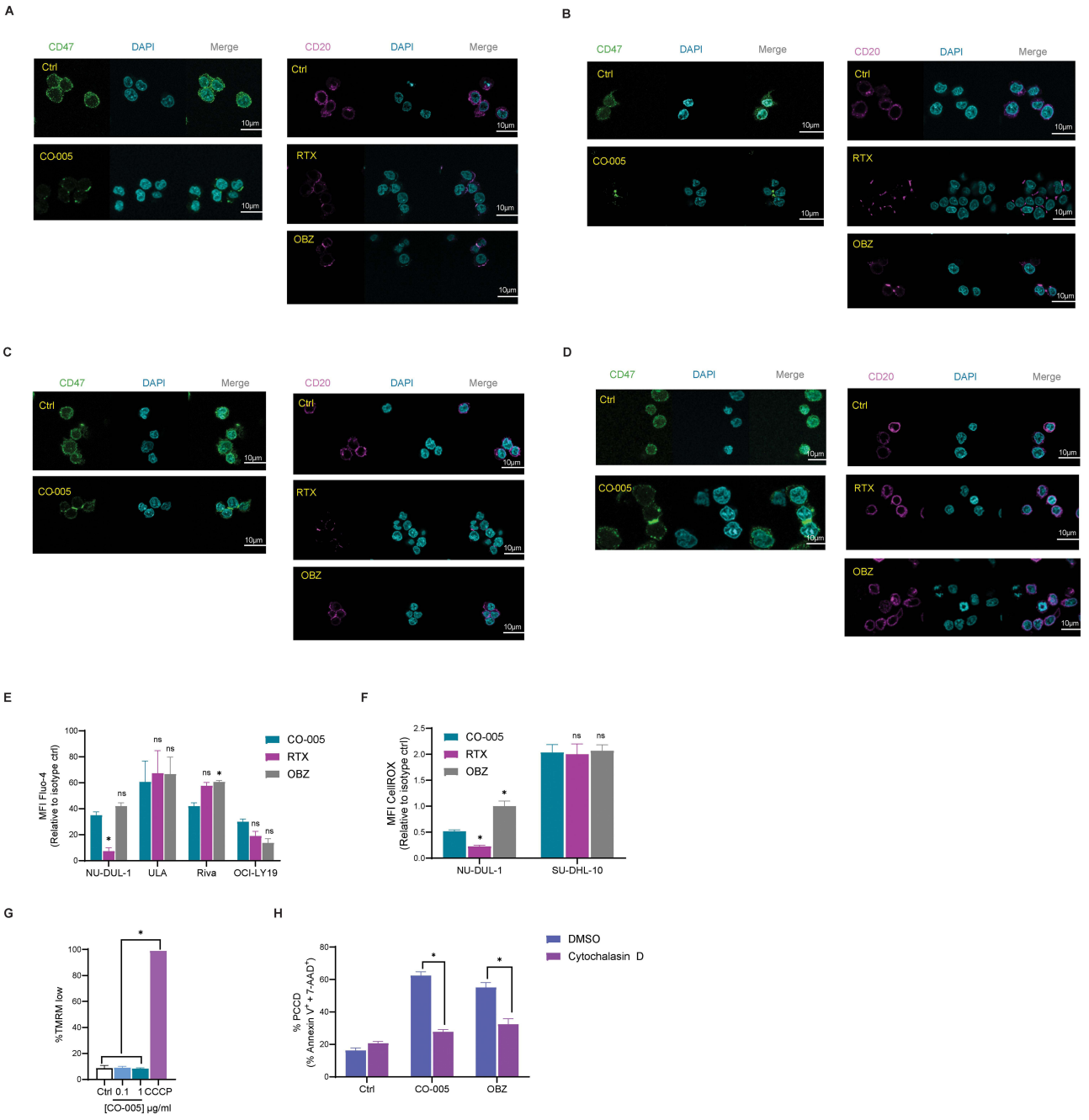

Figure 2 CO-005 triggers receptor capping and intracellular signaling events associated with type II anti-CD20 antibodies. **(A)** NU-DUL-1, **(B)** ULA, **(C)**, SU-DHL-10 and **(D)** OCI-LY19 cells treated with 1 µg/mL CO-005, rituximab (RTX), or obinutuzumab (OBZ) for 3 or 24 hours exhibit distinct patterns of CD47 and CD20 clustering. Receptor distribution was visualized by confocal microscopy following immunofluorescence staining. Scale bar 10 µm. Cellular stress profiling was measured as following **(E)** Intracellular calcium flux in lymphoma cells treated with 1 µg/mL of the indicated antibodies or isotype control for 3 hours, measured by Fluo-4 AM and flow cytometry. **(F)** Reactive oxygen species (ROS) levels following antibody treatment (1 µg/mL, 3 hours), assessed by CellROX Green and flow cytometry. **(G)** Mitochondrial membrane potential (MMP) after CO-005 treatment (0.1 or 1 µg/mL) for 3 hours, determined by TMRM staining. CCCP served as a positive control for mitochondrial depolarization. **(H)** Effect of actin polymerization inhibition on CO-005 – induced cell death following cytochalasin pretreatment (20 µM, 15 min), measured by Annexin V and 7-AAD staining. Data represent the mean ± SD. Significance was determined by ANOVA analysis *, $P < 0.01$ compared to the sample treated with CO-005 or as indicated in the figure; ns indicates not significant. All experiments were performed independently three times (n = 3). MFI, mean fluorescence intensity.

we measured surface exposure of calreticulin by flow cytometry across a panel of DLBCL cell lines lines (NU-DUL-1, ULA, SU-DHL-6, and SU-DHL-10, and Daudi), following treatment with CO-005, RTX, OBZ, or doxorubicin (Doxo) as a positive control. As shown in Figure 3A, CO-005 treatment induced surface calreticulin exposure in multiple DLBCL cell lines, including NU-DUL-1, ULA, SU-DHL-6, SU-DHL-10, and Daudi, at levels comparable to those observed with

 https://doi.org/10.2147/ITT.S572396

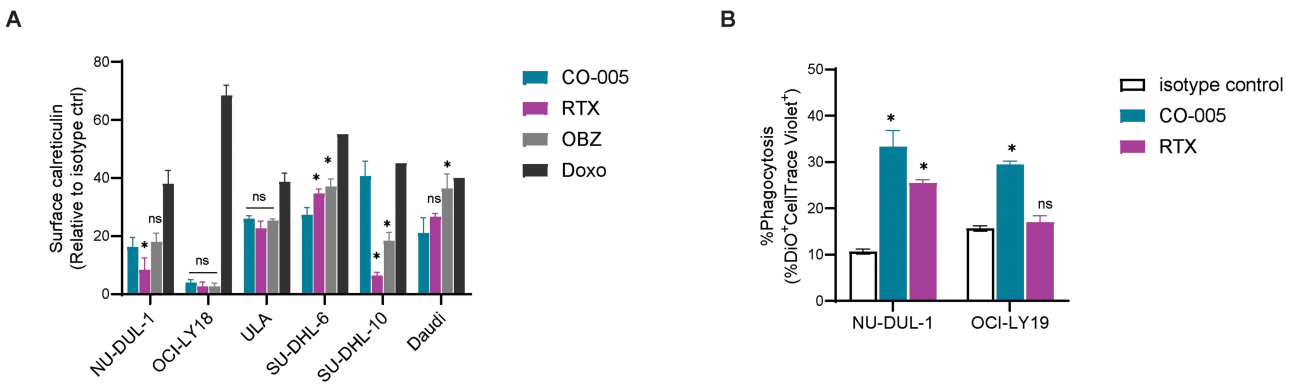

Figure 3 CO-005 shifts the phagocytic balance by enhancing "eat me" and promoting macrophage- mediated clearance. (**A**) Surface Calreticulin exposure was assessed in a panel of lymphoma cell lines (NU-DUL-1, OCI-LY18, ULA, SU-DHL-6, SU-DHL-10 and Daudi) following treatment with CO-005, Rituximab (RTX), or Obinutuzumab (OBZ) for 3 hours; Doxorubicin served as a positive control. Calreticulin expression is shown relative to isotype control. **(B)** Phagocytosis activity of CO-005 or RTX was measured using CellTrace-labeled NU-DUL-1 and OCI-LY19 cells co-cultured with DiO-labeled RAW264.7 macrophages for 2 hours. Phagocytosed cells were quantified as %CellTrace+DiO+ by flow cytometry. Data represent the mean ± SD. Significance was determined by ANOVA analysis *, $P < 0.01$ compared to the sample treated with CO-005; ns indicates not significant. All experiments were performed independently three times (n = 3).

RTX and OBZ, consistent with the induction of PCCD observed in Figure 1B. In contrast, no calreticulin induction was detected in the non-responsive OCI-LY18 cell line following treatment with any of the antibodies, suggesting that surface calreticulin may serve as an early, cell-intrinsic marker of sensitivity to CO-005–mediated PCCD.

To evaluate whether CO-005 enhances the phagocytic clearance of lymphoma, we performed macrophage phagocytosis assays. CellTrace-labeled NU-DUL-1 and OCI-LY19 cells were co-cultured with DiO-labelled macrophages in the presence of CO-005, RTX, or IgG isotype control for 2 hours. As shown in Figure 3B, CO-005 effectively enhanced tumor cell phagocytosis in NU-DUL-1 cells, reaching 32% compared to 10% in the IgG control group and 26% with RTX. In OCI-Ly19 cells, RTX failed to promote phagocytosis, whereas CO-005 achieved a phagocytic rate of 30%, indicating robust engagement despite RTX resistance.

CO-005 Demonstrates Potent Anti-Lymphoma Activity Across Multiple Xenograft Models, Including CD20-Resistant Tumors

To assess the therapeutic efficacy of CO-005 in vivo, we generated three independent human lymphoma xenograft models in NSG mice: NU-DUL-1, a representative ABC-DLBCL line; Daudi, a $CD20^+$ Burkitt lymphoma; and OCI-LY19, a CD20-low/negative DLBCL model resistant to RTX. As illustrated in the study timeline (Figure 4A), mice were randomized into treatment groups once tumor volumes averaged 150 mm^3. Animals received i.p. injections of the treatment twice per week for three weeks. Tumor growth and overall survival were monitored following treatment initiation.

In the NU-DUL-1 xenograft model, CO-005 treatment (5 mg/kg) completely inhibited tumor progression during the treatment period, with all mice maintaining suppressed tumor growth up to Day 55 (Figure 4B, left panel). In contrast, tumors in RTX- and isotype control-treated groups progressed rapidly, with a median survival of 49 days. CO-005 significantly extended survival, with a median of 84 days (Figure 4B, right panel). By Day 100, 2 of 6 mice (33%) in the CO-005 group remained alive with tumor volumes below 300 mm^3, indicating durable antitumor activity following treatment.

In the Daudi xenograft model, we evaluated the efficacy of CO-005 at a subtherapeutic dose (1 mg/kg), a standard dose (5 mg/kg), and in combination with RTX (5 mg/kg). Again, CO-005 at 5 mg/kg inhibited tumor progression with over 90% reduction in tumor volume by day 45, while low-dose CO-005 and RTX monotherapy exhibited limited antitumor activity (Figure 4C, left panel). Notably, the combination of low-dose CO-005 with RTX significantly delayed tumor progression and improved survival relative to either agent alone, indicating an additive benefit (Figure 4C, right panel). Overall, CO-005 demonstrated dose-dependent efficacy, and its combination with RTX resulted in enhanced tumor control.

In the OCI-LY19 model, which expresses minimal CD20 and is resistant to RTX,[28] CO-005 treatment at 5 mg/kg significantly inhibited tumor progression throughout the study period (Figure 4D, left panel). While tumors in both isotype control and RTX-treated mice progressed rapidly. Importantly, all CO-005–treated mice remained alive

https://doi.org/10.2147/ITT.S572396

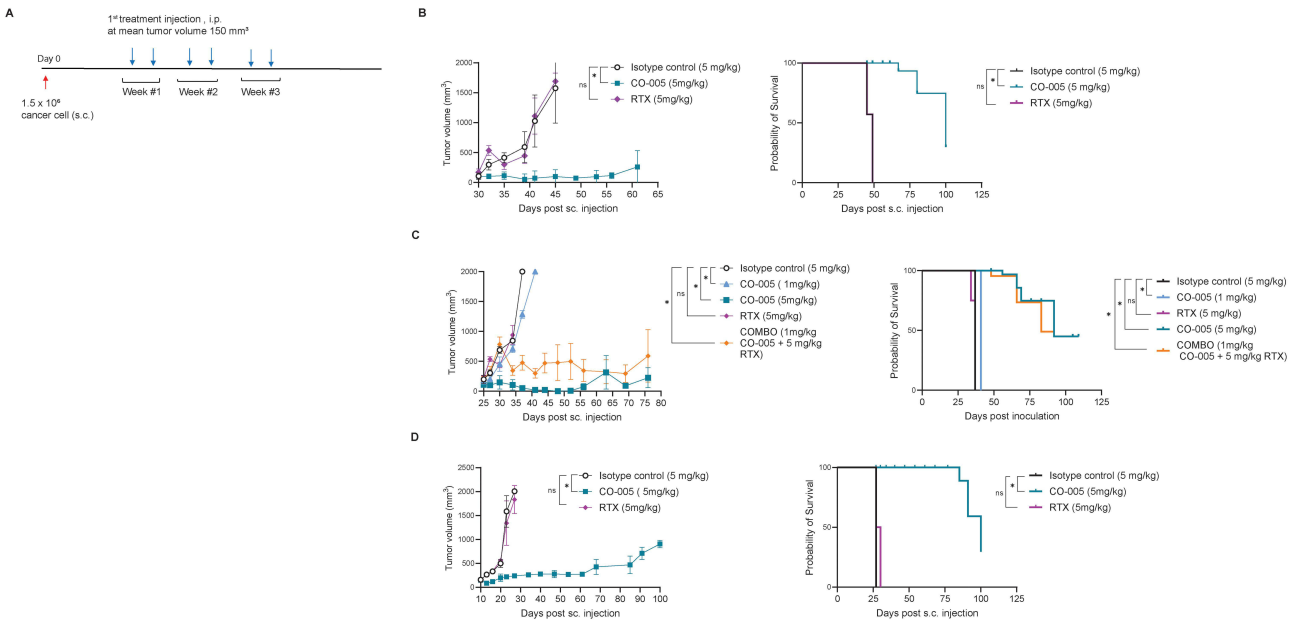

Figure 4 CO-005 demonstrates potent anti-lymphoma activity across multiple xenograft models. **(A)** Experimental timeline for the xenograft study. Mice were inoculated subcutaneously with 1.5 × 10^6 cancer cells (red arrow, Day 0). Treatment injections (blue arrows) were administered intraperitoneally (i.p.) twice weekly, starting when tumors reached a mean volume of 150 mm^3, for a total of three weeks. **(B–D)** Tumor growth (left) and survival (right) outcomes in three xenograft models: NU-DUL-1 **(B)**: Mice were treated with CO-005 (5 mg/kg), RTX (5 mg/kg), or isotype control (5 mg/kg), *n*= 6. Daudi **(C)**: Mice received CO-005 at 1 mg/kg or 5 mg/kg, RTX at 5 mg/kg, or a combination of CO-005 (1 mg/kg) and RTX (5 mg/kg), or isotype control (5 mg/kg), n= 5. OCI-LY19 **(D)**: Mice were treated with CO-005 (5 mg/kg), RTX (5 mg/kg), or isotype control (5 mg/kg), n= 6. Tumor volumes were measured biweekly by caliper and calculated as (length × $width^2$)/2. Data represents the mean ± S.D, *p<0.01 (Mann–Whitney *U*-test), compared to the sample treated with Isotype control at the indicated day (endpoint before control animals are sacrificed); ns indicates not significant. n= animals per treatment group. Survival was monitored until the end of study, *p<0.01 (log-rank (Mantel- Cox) test.

beyond day 80, whereas complete mortality was observed in RTX and control group by day 35 (Figure 4D, right panel). Notably, by day 100, two mice in the CO-005 group remained alive with no signs warranting euthanasia, indicating durable tumor control. The experiment was concluded at this time due to study endpoint constraints, rather than any observed decline in animal health. These findings highlight the potential of CO-005 to deliver sustained therapeutic benefit in RTX-refractory or CD20-deficient lymphomas, where conventional anti-CD20 therapies are ineffective.

CO-005 Induces PCCD in Vivo and Modulates the Tumor Immune Microenvironment

To further investigate the contribution of PCCD to the antitumor activity of CO-005 and its impact on the tumor microenvironment, we conducted a short-term mechanistic study in a Raji xenograft model (Figure 5A). Following standard engraftment protocols, mice were treated with a single dose of CO-005 (5 mg/kg, i.p) or isotype control on day 10 post inoculation. Three days later (day 13), tumors were measured and were subsequently harvested for flow cytometric analysis, as shown in Figure 5B, CO-005 treatment resulted in a significant reduction in tumor volume compared to isotype control. Importantly, this rapid tumor regression was accompanied by a substantial increase in Annexin V and 7-AAD double positive cells (Figure 5C), indicative of cell death within the remaining tumor. Although NSG mice are severely immunodeficient, including compromised macrophage function and lack of functional T and B cells, they retain residual innate immune compartments such as neutrophils and some macrophage subsets.[33] As shown in Figure 5D, significant increase in $F4/80^+$ macrophages in CO-005–treated tumors. Notably, CO-005 also increased the infiltration of $Ly6G^+$ neutrophils (Figure 5E).

Discussion

CD20-targeted immunotherapies have revolutionized the treatment of B-cell malignancies, but resistance and relapse remain significant challenges.[1,21] These limitations often stem from antigen loss, immune evasion, or impaired effector function—particularly in aggressive or refractory disease.[34] This study introduces CO-005, a bivalent humanized anti-

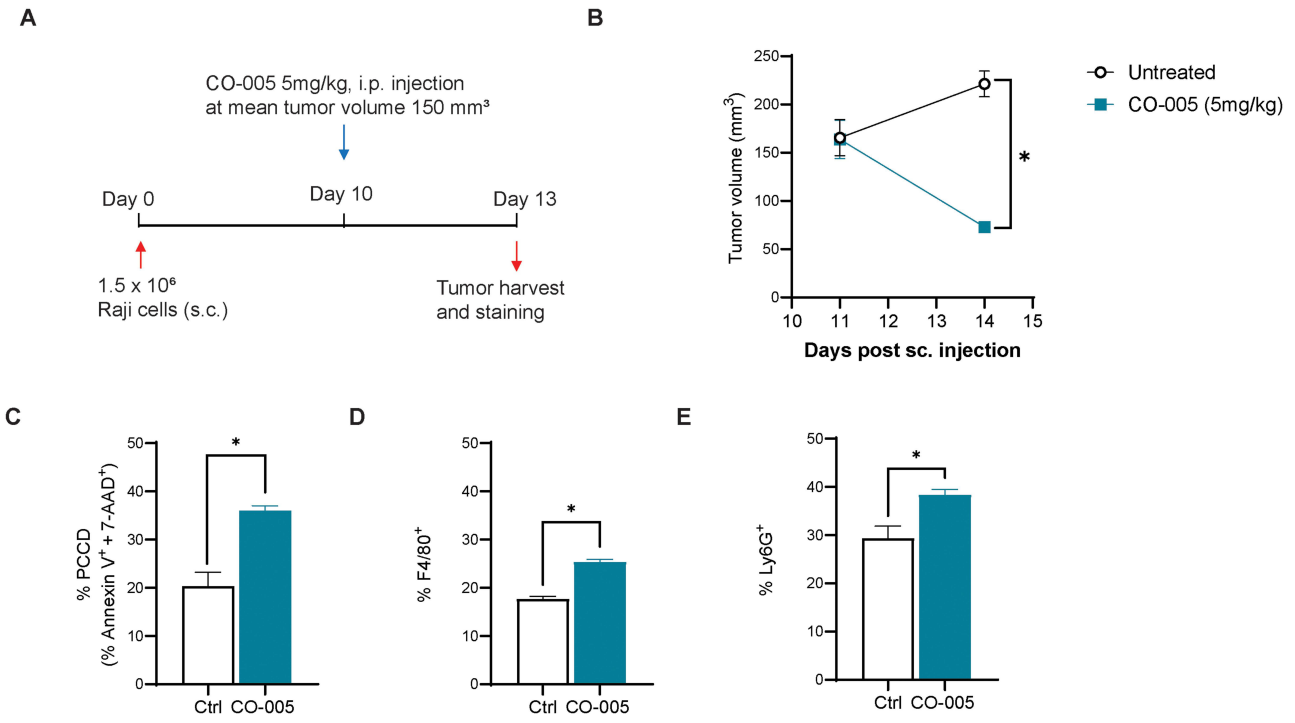

Figure 5 CO-005 induces PCCD in vivo and promotes innate immune cell infiltration in a Raji xenograft model. **(A)** Experimental timeline for dosing and tumor harvest for single-cell analysis. Mice were inoculated subcutaneously with 1.5 × 10^6 Raji cells (red arrow, Day 0). Treatment injections (blue arrows) were administered intraperitoneally (i.p.) at Day 10, and tumors were harvested at Day 13 (red arrow) **(B)** Tumor volumes measured before treatment and at harvest. **(C–E)** Flow cytometric analysis of tumor dissociates: **(C)** Apoptotic tumor cells (human $CD20^+$, Annexin V/7-AAD^+), **(D)** Murine macrophage infiltration ($F4/80^+$), and **(E)** neutrophil infiltration ($Ly6G^+$). Innate immune cell infiltration is shown as a percentage shift relative to isotype controls. Data represent mean ± SD; *p < 0.01 vs isotype control (unpaired two-tailed Student's *t*-test); ns indicates not significant. n = 3 mice per group.

CD47 scFv-Fc fusion protein, as a mechanistically distinct approach capable of overcoming key constraints of CD20-based B cell lymphoma therapies.

CO-005 combines checkpoint inhibition with direct immunogenic cytotoxicity, offering an alternative to agents that rely solely on Fc-mediated phagocytosis.[14,35] While previous studies have linked anti-CD47 antibodies to non-apoptotic cell death, the upstream signaling events have been incompletely defined.[36–38] Here, we show that CO-005 induces fast and potent form of cell death,[14] marked by receptor capping, calcium flux, actin remodeling, and phosphatidylserine exposure. These features parallel those observed with anti-CD20 antibodies such as RTX and OBZ yet occur independently of CD20 expression or Fc engagement.[16,31,39] CD47 capping appears to play a central role in CO-005–mediated cell death. This rapid redistribution of CD47 is observed specifically in PCCD-responsive cells and is absent in cells treated with anti-CD47 antibodies such as magrolimab or B6H12 that have no direct killing mechanism.[35,40–42] The selective capping pattern likely reflects a structural consequence of the CO-005–CD47 interaction. These findings support the emerging concept that CD47 functions not only as an inhibitory "don't eat me" signal but also as a membrane-integrated signaling platform when engaged in a specific manner. Similar receptor reorganization has been reported with rituximab, where CD20 capping facilitates immunological synapse formation with NK cells. Similarly, CD47 clustering may promote immune cell engagement while concurrently triggering intracellular death signaling.[29] Notably, CO-005–induced PCCD proceeds apparently independently of mitochondrial pathways. While ROS generation was observed, mitochondrial membrane potential remained intact, aligning with prior evidence that CD47-triggered ROS is NADPH oxidase–driven rather than mitochondria-derived.[16,31] In contrast, calcium flux was rapid and reproducible in responsive cells, suggesting that calcium acts not only as a signal amplifier but also as a potential biomarker of CO-005 activity. Further testing in a broader set of primary lymphoma samples and cell lines is needed to strengthen its potential as a generalizable marker of CO-005 activity. In our study, CO-005 triggered PCCD in some cells from both ABC and GCB DLBCL subtypes, consistent with comparable CD47 expression and indicating that subtype alone is unlikely to dictate

https://doi.org/10.2147/ITT.S572396

responsiveness. Nevertheless, patient-specific factors, including immune context and tumor heterogeneity, may influence therapeutic outcomes in clinical settings. Expanding evaluation to diverse patient-derived samples will be important to identify determinants of response and guide personalized application of CO-005.

Beyond its cytotoxic activity, CO-005 may also be prime elements of the tumor-immune interface. The surface exposure of immunogenic DAMP-like signals, including phosphatidylserine and calreticulin, was associated with innate immune cell infiltration even in NSG mice with limited effector cell function.[33] While antibody-induced immunogenic cell death remains rare, these findings suggest that CO-005 may act as both an effector and immune modulator.[17,43] Importantly, the rapid CD47 reorganization on tumor cells and cell death signaling observed in vitro likely underlie these in vivo immune effects, linking tumor-intrinsic events to enhanced recognition and recruitment of innate immune cells.

The potent antitumor activity of CO-005 across multiple DLBCL xenograft models, highlights its potential to overcome CD20- loss resistance mechanisms, that commonly limit the efficacy of CD20-targeted therapies. Its activity in both CD20-positive and CD20-low settings reflects its therapeutic relevance in relapsed or refractory disease. Mechanistically, CO-005 combines direct PCCD with innate immune activation, recapitulating key features of chemoimmunotherapy cytotoxicity and immune engagement within a single agent, and offering a chemotherapy-free alternative for patients who are ineligible for or unresponsive to standard regimens.[2] Although the activity of rituximab in NSG mice is sometimes debated due to the absence of NK cells and complement, published data have demonstrated that macrophages are sufficient to mediate therapeutic effects in this model, lending support to the additive benefit observed in our combination studies.[19]

Conclusion

This study defines CO-005 as a mechanistically unique anti-CD47 therapeutic that not only blocks immune evasion but initiates a rapid, structured form of PCCD associated with further activation of the immune system. Characterizing the molecular and gene expression profiles associated with PCCD responsiveness could serve as a functional biomarker to distinguish responsive from non-responsive tumors, enabling a more personalized approach to treatment. By mimicking and extending the mechanistic features of anti-CD20 antibodies, while bypassing their antigenic and effector dependencies, CO-005 may offer a new path forward in the treatment of B-cell lymphoma.

Abbreviations

ABC, activated B-cell–like; AM,acetoxymethyl ester; ANOVA, analysis of variance; ATCC, American Type Culture Collection; 7-AAD, 7-aminoactinomycin D; BSA, bovine serum albumin; CD, Cluster of differentiation; DAMP, Damage-Associated Molecular Patterns; DLBCL, diffuse large B-cell lymphoma; DMEM, Dulbecco's Modified Eagle Medium; DSMZ, Leibniz Institute DSMZ–German Collection of Microorganisms and Cell Cultures; EDTA, ethylenediaminetetraacetic acid; ER, Endoplasmic Reticulum; FBS, fetal bovine serum; Fc, fragment crystallizable; GCB, germinal center B-cell–like; IMDM, Iscove's Modified Dulbecco's Medium; HBSS, hanks balanced salt solution; HEP, humane end point; IT, intratibial; IP, intra-peritoneal; mAb, monoclonal antibody; MMP, mitochondrial membrane potential; MOPC-1, mouse IgG1 chimeric isotype control; NSG, NOD scid IL2Rγnull; OBZ, Obinutuzumab; PBMC, peripheral blood mononuclear cells; PBS, Phosphate-Buffered Saline; PE, phycoerythrin; PFA, paraformaldehyde; PS, phosphatidylserine; PCCD, programmed cancer cell death; RBC, red blood cell; R-CHOP, rituximab, cyclophosphamide, doxorubicin, vincristine, and prednisone; RTX, rituximab; ROS, reactive oxygen species scFv, single-chain fragment variable; SC, subcutaneous; SD, standard deviation; SIRPα, signal regulatory protein alpha; TMRM, tetramethylrhodamine methyl ester.

Data Sharing Statement

The data that support the findings of this study are available from the corresponding author upon reasonable request.

Acknowledgments

We thank Associate Professor and Group Leader Alexandre Corthay (Medical Division, Laboratory Medicine, Department of Pathology, Oslo University Hospital) and colleagues Inger Øynebråten and Karen Irion for their valuable advice and support during this study.

Funding

The study was funded by Caedo Oncology AS.

Disclosure

S.M., S.S., L.E.B.M., and N.R. are employees of Caedo Oncology. K.H., Ø.Å., and R.D.P. hold consulting or advisory roles in Caedo Oncology. K.H. and R.D.P. hold stocks and ownership interests in Caedo Oncology. S.M., S.S., K.H., R.D.P., N.R. have patents WO202407472A1 and WO2024074730A2 pending related to this work. H.R.H. declare no competing financial interests.

The authors report no other conflicts of interest in this work.

References

1. Casan JML, Wong J, Northcott MJ, Opat S. Anti-CD20 monoclonal antibodies: reviewing a revolution. *Hum Vaccin Immunother*. 2018;14 (12):2820–2841. doi:10.1080/21645515.2018.1508624
2. Tavarozzi R, Zacchi G, Pietrasanta D, et al. Changing trends in B-cell non-hodgkin lymphoma treatment: the role of novel monoclonal antibodies in clinical Practice. *Cancers*. 2023;15(22):5397. doi:10.3390/cancers15225397
3. Sehn LH, Salles G, Longo DL. Diffuse large B-cell lymphoma. *N Engl J Med*. 2021;384(9):842–858. doi:10.1056/NEJMra2027612
4. Beers SA, French RR, Chan HTC, et al. Antigenic modulation limits the efficacy of anti-CD20 antibodies: implications for antibody selection. *Blood*. 2010;115(25):5191–5201. doi:10.1182/blood-2010-01-263533
5. Schuster SJ, Huw L-Y, Bolen CR, et al. Loss of CD20 expression as a mechanism of resistance to mosunetuzumab in relapsed/refractory B-cell lymphomas. *Blood*. 2024;143(9):822–832. doi:10.1182/blood.2023022348
6. Weiner LM, Surana R, Wang S. Monoclonal antibodies: versatile platforms for cancer immunotherapy. *Nat Rev Immunol*. 2010;10(5):317–327. doi:10.1038/nri2744
7. Smith MR. Rituximab (monoclonal anti-CD20 antibody): mechanisms of action and resistance. *Oncogene*. 2003;22(47):7359–7368. doi:10.1038/sj.onc.1206939
8. Johnson NA, Boyle M, Bashashati A, et al. Diffuse large B-cell lymphoma: reduced CD20 expression is associated with an inferior. *Blood*. 2009;16(1).
9. Lao Y, Shen D, Zhang W, He R, Jiang M. Immune checkpoint inhibitors in cancer therapy-how to overcome drug resistance? *Cancers*. 2022;14 (15):3575. doi:10.3390/cancers14153575
10. Leclair P, Lim CJ. CD47 (cluster of differentiation 47): an anti-phagocytic receptor with a multitude of signaling functions. *Anim Cells Syst*. 2020;24(5):243–252. doi:10.1080/19768354.2020.1818618
11. Matlung HL, Szilagyi K, Barclay NA, van den Berg TK. The CD47-SIRPα signaling axis as an innate immune checkpoint in cancer. *Immunol Rev*. 2017;276(1):145–164. doi:10.1111/imr.12527
12. Oldenborg P-A, Zheleznyak A, Fang Y-F, Lagenaur CF, Gresham HD, Lindberg FP. Role of CD47 as a marker of self on red blood cells. *Science*. 2000;288(5473):2051–2054. doi:10.1126/science.288.5473.2051
13. Xu Y, Jiang P, Xu Z, Ye H. Opportunities and challenges for anti-CD47 antibodies in hematological malignancies. *Front Immunol*. 2024;15 (1348852). doi:10.3389/fimmu.2024.1348852
14. Matar S, Skah S, Diomande LE, et al. Development of a novel bifunctional anti-CD47 fusion protein with improved efficacy and a favorable safety profile. *Mol Cancer Ther*. 2025;24(6):816–827. doi:10.1158/1535-7163.MCT-24-0917
15. Dalle S, Reslan L, Besseyre de Horts T, et al. Preclinical studies on the mechanism of action and the anti-lymphoma activity of the novel anti-CD20 antibody GA101. *Mol Cancer Ther*. 2011;10(1):178–185. doi:10.1158/1535-7163.MCT-10-0385
16. Honeychurch J, Alduaij W, Azizyan M, et al. Antibody-induced nonapoptotic cell death in human lymphoma and leukemia cells is mediated through a novel reactive oxygen species-dependent pathway. *Blood*. 2012;119(15):3523–3533. doi:10.1182/blood-2011-12-395541
17. Cheadle EJ, Sidon L, Dovedi SJ, et al. The induction of immunogenic cell death by type II anti- CD 20 monoclonal antibodies has mechanistic differences compared with type I rituximab. *Br J Haematol*. 2013;162(6):842–845. doi:10.1111/bjh.12427
18. Piccione EC, Juarez S, Liu J, et al. A bispecific antibody targeting CD47 and CD20 selectively binds and eliminates dual antigen expressing lymphoma cells. *MAbs*. 2015;7(5):946–956. doi:10.1080/19420862.2015.1062192
19. Chao MP, Alizadeh AA, Tang C, et al. Anti-CD47 antibody synergizes with rituximab to promote phagocytosis and eradicate non-Hodgkin lymphoma. *Cell*. 2010;142(5):699–713. doi:10.1016/j.cell.2010.07.044
20. Cho J, Yoon SE, Kim SJ, Ko YH, Kim WS. CD47 overexpression is common in intestinal non-GCB type diffuse large B-cell lymphoma and associated with 18q21 gain. *Blood Adv*. 2022;6(24):6120–6130. doi:10.1182/bloodadvances.2021006305
21. Kubacz M, Kusowska A, Winiarska M, Bobrowicz M. In vitro diffuse large B-cell lymphoma cell line models as tools to investigate novel immunotherapeutic strategies. *Cancers*. 2022;15(1):235. doi:10.3390/cancers15010235
22. Schneider CA, Rasband WS, Eliceiri KW. NIH Image to ImageJ: 25 years of image analysis. *Nat Methods*. 2012;9(7):671–675. doi:10.1038/nmeth.2089
23. Zhang Y-Q, Shen X, Xiao X-L, et al. Mitochondrial uncoupler carbonyl cyanide m-chlorophenylhydrazone induces vasorelaxation without involving K ATP channel activation in smooth muscle cells of arteries. *Br J Pharmacol*. 2016;173(21):3145–3158. doi:10.1111/bph.13578
24. Ribeiro ML, Profitós-Pelejà N, Santos JC, et al. GPR183 mediates the capacity of the novel CD47-CD19 bispecific antibody TG-1801 to heighten ublituximab-umbralisib (U2) anti-lymphoma activity. *bioRxiv*. 2022:2022–03. doi:10.1101/2022.03.31.486558
25. Yanguas-Casás N, Pedrosa L, Fernández-Miranda I, Sánchez-Beato M. An overview on diffuse large B-cell lymphoma models: towards a functional genomics approach. *Cancers*. 2021;13(12):2893. doi:10.3390/cancers13122893
26. Bouwstra R, He Y, de BJ, et al. CD47 expression defines efficacy of rituximab with CHOP in non-germinal center B-cell (Non-GCB) diffuse large B-cell lymphoma patients (DLBCL). *but Not in GCB DLBCL Cancer Immunol Res*. 2019;7(10):1663–1671. doi:10.1158/2326-6066.CIR-18-0781

27. Herter S, Herting F, Mundigl O, et al. Preclinical activity of the type II CD20 antibody GA101 (obinutuzumab) Compared with rituximab and ofatumumab in vitro and in xenograft models. *Mol Cancer Ther*. 2013;12(10):2031–2042. doi:10.1158/1535-7163.MCT-12-1182
28. Daniel D, Yang B, Lawrence DA, et al. Cooperation of the proapoptotic receptor agonist rhApo2L/TRAIL with the CD20 antibody rituximab against non-Hodgkin lymphoma xenografts. *Blood*. 2007;110(12):4037–4046. doi:10.1182/blood-2007-02-076075
29. Rudnicka D, Oszmiana A, Finch DK, et al. Rituximab causes a polarization of B cells that augments its therapeutic function in NK-cell–mediated antibody-dependent cellular cytotoxicity. *Blood*. 2013;121(23):4694–4702. doi:10.1182/blood-2013-02-482570
30. Vacher P, Vacher A-M, Pineau R, et al. Localized store-operated calcium influx represses CD95-dependent apoptotic effects of rituximab in non-Hodgkin B LYMPHOMAS. *J Immunol*. 2015;195(5):2207–2215. doi:10.4049/jimmunol.1402942
31. Latour S, Zanese M, Le Morvan V, et al. Role of calcium signaling in GA101-induced cell death in malignant human B cells. *Cancers*. 2019;11(3):291. doi:10.3390/cancers11030291
32. Gardai SJ, McPhillips KA, Frasch SC, et al. Cell-surface calreticulin initiates clearance of viable or apoptotic cells through trans-activation of LRP on the phagocyte. *Cell*. 2005;123(2):321–334. doi:10.1016/j.cell.2005.08.032
33. Chen J, Liao S, Xiao Z, et al. The development and improvement of immunodeficient mice and humanized immune system mouse models. *Front Immunol*. 2022;13(1007579). doi:10.3389/fimmu.2022.1007579
34. Dabkowska A, Domka K, Firczuk M. Advancements in cancer immunotherapies targeting CD20: from pioneering monoclonal antibodies to chimeric antigen receptor-modified T cells. *Front Immunol*. 2024;15(1363102). doi:10.3389/fimmu.2024.1363102
35. Liu J, Wang L, Zhao F, et al. Pre-clinical development of a humanized Anti-CD47 antibody with anti-cancer therapeutic potential. *PLoS One*. 2015;10(9):e0137345. doi:10.1371/journal.pone.0137345
36. Puro RJ, Bouchlaka MN, Hiebsch RR, et al. Development of AO-176, a next-generation humanized Anti-CD47 Antibody with novel anticancer properties and negligible red blood cell binding. *Mol Cancer Ther*. 2020;19(3):835–846. doi:10.1158/1535-7163.MCT-19-1079
37. Pettersen RD, Hestdal K, Olafsen MK, Lie SO, Lindberg FP. CD47 signals T cell death. *J Immunol*. 1999;162(12):7031–7040.
38. Leclair P, Liu -C-C, Monajemi M, Reid GS, Sly LM, Lim CJ. CD47-ligation induced cell death in T-acute lymphoblastic leukemia. *Cell Death Dis*. 2018;9(5):544. doi:10.1038/s41419-018-0601-2
39. Alduaij W, Ivanov A, Honeychurch J, et al. Novel type II anti-CD20 monoclonal antibody (GA101) evokes homotypic adhesion and actin-dependent, lysosome-mediated cell death in B-cell malignancies. *Blood*. 2011;117(17):4519–4529. doi:10.1182/blood-2010-07-296913
40. Advani R, Flinn I, Popplewell L, et al. CD47 blockade by Hu5F9-G4 and rituximab in non-Hodgkin's lymphoma. *N Engl J Med*. 2018;379(18):1711–1721. doi:10.1056/NEJMoa1807315
41. Bouwstra R, van Meerten T, Bremer E. CD47-SIRPα blocking-based immunotherapy: current and prospective therapeutic strategies. *Clin Transl Med*. 2022;12(8):e943. doi:10.1002/ctm2.943
42. Lin F, Xiong M, Hao W, et al. A novel blockade CD47 antibody with therapeutic potential for cancer. *Front Oncol*. 2020;10(615534). doi:10.3389/fonc.2020.615534
43. Galluzzi L, Kepp O, Hett E, Kroemer G, Marincola FM. Immunogenic cell death in cancer: concept and therapeutic implications. *J Transl Med*. 2023;21(1):162. doi:10.1186/s12967-023-04017-6